

Horizon instability of massless scalar perturbations of an extreme Reissner-Nordström-AdS black hole

Shao-Jun Zhang¹, Qiyuan Pan², Bin Wang¹, Elcio Abdalla³

¹*Department of Physics and Astronomy, Shanghai Jiao Tong University, Shanghai 200240, China*

²*Institute of Physics and Department of Physics,
Hunan Normal University, Changsha, Hunan 410081, China*

³*Instituto de Física, Universidade de São Paulo,
C.P.66.318, CEP 05315-970, São Paulo, Brazil*

(Dated: February 26, 2022)

We study the stability of extreme Reissner-Nordström-AdS black hole under massless scalar perturbations. We show that the perturbation on the horizon of the extreme Reissner-Nordström-AdS black hole experiences a power-law decay, instead of an exponential decay as observed in the nonextreme AdS black hole. On the horizon of the extreme Reissner-Nordström-AdS black hole, the blow up happens at lower order derivative of the scalar field compared with that of the extreme Reissner-Nordström black hole, which shows that extreme AdS black holes tend to instability in comparison to black holes in asymptotic flat space-times.

PACS numbers: 04.70.Bw, 04.25.-g, 98.80.Es

I. INTRODUCTION

The black hole, an exotic astronomical object predicted in general relativity, is playing more and more important roles in various fields of modern physics. Showing the existence of such an object by studying its stability is obviously important. Starting from the influential study by Regge and Wheeler [1], the stability of black holes has been investigated over half a century. It has been demonstrated that most black holes are stable under various types of perturbations (for a recent review see for example [2]), which shows that the black hole is realizable in practice and is not just a mathematical curiosity.

Recently, Aretakis carefully examined the stability of the extreme black holes in the asymptotically flat spacetime. They proved analytically that for the extreme Reissner-Nordström (eRN) and Kerr (eKerr) black holes, there exists a classical instability under massless scalar field perturbations [3–6].

This is an amazing result viewed from two aspects. The first one is that non-extreme RN and

Kerr black holes are stable against massless scalar field perturbations [7, 8], so it is surprising that the stability of black holes changes radically when the extremal limit is approached. The second one is that extreme black hole occupies an essential place in understanding quantum theory of gravity. For example, the Bekenstein-Hawking entropy of extremal supersymmetric black holes can have statistical explanation in string theory [9, 10], which reflects a quantum aspect of gravity. The study on the stability of extreme black holes is obviously important. Aretakis' result suggests that the stability of extreme black holes has to be reexamined.

Aretakis' argument can be briefly summarized as follows. We work in the ingoing Eddington-Finkelstein (EF) coordinates v and r , and suppose that the initial data for the perturbation ψ is defined on a spacelike surface intersecting with the future horizon and further, one can construct a certain conserved quantity on the horizon, i.e., the so-called Aretakis constant. With this constant, it can be proved analytically that the derivative $\partial_r \psi$ shall not decay on the horizon. However, the field itself, ψ does decay on the horizon as well as outside. Moreover, all radial derivatives of ψ fall off outside the horizon. The non-decay of $\partial_r \psi$ on the horizon leads to a blow up of $\partial_r^2 \psi$ on the horizon at late times. Aretakis could demonstrate that the derivative $\partial_r^k \psi$ blows up at the horizon as v^{k-1} or even faster. This suggests the instability of the extreme black hole. This proof was extended to other extreme black holes in the asymptotically flat spacetime in various dimensions [11]. Similar instability was also found in the electromagnetic and gravitational perturbations in the eKerr black hole [11]. This type of gravitational instability was also observed for higher dimensional extreme black holes [12].

Aretakis's analytic argument was recently confirmed in [13] by a numerical calculation. They examined the late time behavior of the scalar field in great detail and found that in the asymptotically flat spacetime the mode of the massless scalar perturbations with higher l (where l is the spherical harmonic index) decays faster. They also discussed the case provided that one can not define the non-zero Aretakis constant where Aretakis' analytical argument breaks down and found that the horizon instability still exists (see also the recent work [14, 15] where an analytical argument is given for this case). Moreover, they showed that for a massive scalar field as well as for electromagnetic and gravitational perturbations, an instability also develops.

In this paper, we will extend the study to the extreme Reissner-Nordström (eRN-AdS) black hole. Motivated by the recent discovery of the AdS/CFT correspondence, the investigation of the stability of AdS black holes becomes more appealing. The stability of the nonextreme AdS black holes has been studied extensively, see for example [2] and references therein. In the nonextreme AdS black hole, it was shown that the behavior of perturbations differs a lot from those in the

asymptotically flat spacetimes. For example, the scalar field experiences an exponential decay at late time in the AdS black hole background [16–18] instead of a power-law decay in the asymptotically flat black holes [19–22]. Higher l modes will experience an increase of the damping time scale and a decrease of the oscillation time scale compared with the lower l modes in the AdS black hole [18, 23–25], while the situation is opposite in the asymptotically flat black hole [20]. These differences in the behaviors of perturbations are caused by the different effective potentials and boundary conditions in the AdS black hole compared with the asymptotically flat black hole. Here we want to examine how the presence of the negative cosmological constant affects the stability of extreme black holes in the AdS space. We will focus on the massless scalar field perturbations. In [25], it was argued that when the RN-AdS black hole approaches to the extremal limit, the late time decay of the scalar field outside the black hole changes from exponential to power-law. It is interesting to check this result in the exactly extreme RN-AdS black hole background both outside the horizon and on the horizon. We will examine the stability of the extreme RN-AdS black hole and compare the result with that in the asymptotically flat black holes.

This paper is organized as follows. In section II, we will follow Aretakis' argument to study the horizon stability of eRN-AdS black hole analytically. In section III, we will use numerical method to study the behavior of the massless scalar field perturbations for different angular index $l = 0, 1$ and 2, respectively. Section IV is devoted to conclusion and discussion. In order to compare with the eRN case, we will set all parameters to be the same as in [13].

II. HORIZON INSTABILITY: ANALYTICAL RESULTS

In this section, we will follow Aretakis' argument [3–6] to study the stability of extremal RN-AdS black hole under massless scalar perturbations analytically. The metric of the extremal RN-AdS black hole takes the form

$$\begin{aligned}
 ds^2 &= -f(r)dt^2 + f^{-1}(r)dr^2 + r^2d\Omega^2 \quad , \\
 f(r) &= \frac{1}{R^2r^2} (r^2 + 2r_+r + R^2 + 3r_+^2) (r - r_+)^2 \quad ,
 \end{aligned}
 \tag{1}$$

where r_+ denotes the degenerate horizon, and R is the AdS radius related to the cosmological constant Λ by $\Lambda = -3/R^2$. The tortoise coordinate is

$$\begin{aligned} r_*(r) &= \int \frac{dr}{f(r)} \\ &= \frac{R^2}{(R^2 + 6r_+^2)^2} \left[-\frac{r_+^2 (R^2 + 6r_+^2)}{r - r_+} + \frac{R^4 + 7R^2 r_+^2 + 14r_+^4}{\sqrt{R^2 + 2r_+^2}} \arctan \left(\frac{r + r_+}{\sqrt{R^2 + 2r_+^2}} \right) \right. \\ &\quad \left. + 2r_+ (R^2 + 4r_+^2) \log(r - r_+) - r_+ (R^2 + 4r_+^2) \log(r^2 + 2rr_+ + 3r_+^2 + R^2) \right]. \end{aligned} \quad (2)$$

With the ingoing Eddington-Finkelstein (EF) coordinates, the metric becomes

$$ds^2 = -f(r)dv^2 + 2dvdr + r^2 d\Omega^2, \quad (3)$$

where $v = t + r_*$.

The dynamics of the massless scalar perturbation is governed by the Klein-Gordon equation

$$\nabla^2 \psi = 0. \quad (4)$$

Working in the EF coordinate (3), we begin by expanding ψ as

$$\psi(v, r, \Omega) = \sum_{l=0}^{\infty} \psi_l(v, r) Y_l(\Omega), \quad (5)$$

where the index m has been dropped. Substituting it into the equation of motion, we obtain

$$2r\partial_v \partial_r (r\psi_l) + \partial_r (\Delta \partial_r \psi_l) - l(l+1)\psi_l = 0, \quad (6)$$

where $\Delta = \frac{1}{R^2} (r^2 + 2r_+ r + R^2 + 3r_+^2) (r - r_+)^2$. We work with zero angular momentum ($l = 0$) and compute the expression at $r = r_+$. We can thus show that

$$H_0[\psi] \equiv \frac{1}{r_+} [\partial_r (r\psi_0)]_{r=r_+}, \quad (7)$$

is independent of v .

The constant H_0 does not vanish for general initial data, thus remaining non-zero. As a consequence the field and its radial derivative do not simultaneously tend to zero at the horizon. Later, we show how ψ decays at late times using a numerical computation. Therefore, $\partial_r \psi$ does not decay at the horizon,

$$(\partial_r \psi_0)_{r=r_+} \rightarrow H_0 \quad \text{as} \quad v \rightarrow \infty. \quad (8)$$

Now, acting on (6) with ∂_r for $l = 0$ and $r = r_+$, we obtain

$$\left[\partial_v \partial_r^2 (r\psi_0) + \left(\frac{6}{R^2} + \frac{1}{r_+} \right) \partial_r \psi_0 \right]_{r=r_+} = 0 \quad . \quad (9)$$

Hence,

$$[\partial_v \partial_r^2 (r\psi_0)]_{r=r_+} \rightarrow - \left(\frac{6}{R^2} + \frac{1}{r_+} \right) H_0 \quad \text{as} \quad v \rightarrow \infty \quad . \quad (10)$$

This result leads to the fact that the second radial derivative of the field diverges for large v at the horizon, (similar conclusion being true for higher derivatives, as one can easily see deriving (6))

$$(\partial_r^2 \psi_0)_{r=r_+} \sim - \left(\frac{6}{r_+ R^2} + \frac{1}{r_+^2} \right) H_0 v \quad \text{as} \quad v \rightarrow \infty \quad . \quad (11)$$

Such instability is typical for $l = 0$ perturbations. For $l > 0$, because of the complexity of Δ in (6), we can not define a conserved Aretakis constant by taking ∂_r^l on the equation of motion (6) and evaluating it at the horizon as in the eRN case [13]. Thus, in contrast with the eRN case [13], the above analytic analysis cannot be extended to arbitrary $l > 0$.

However, for $l > 0$ modes, we can still get some important information by analyzing the asymptotical property of the equation of motion (6) at large v by supposing that the late-time behavior of $\phi \equiv r\psi_l$ on the horizon is about v^{a_0} with a_0 a negative non-integer constant. We will prove this assumption and get a_0 later using numerical method. Then from (6), at large v , we get that $\partial_r \phi|_{r=r_+} \sim v^{a_0+1}$. By taking further r -derivatives of (6), and analyzing the behavior at large v , we can obtain

$$\partial_r^n \phi|_{r=r_+} \sim v^{a_0+n} \quad \text{as} \quad v \rightarrow \infty. \quad (12)$$

This implies that there is always horizon instability for large enough n .

III. NUMERICAL RESULTS FOR MASSLESS SCALAR PERTURBATIONS

In this section, we use a numerical method to analyze the behavior of the massless scalar perturbations along the horizon in the background of the eRN-AdS black hole. In the analytic analysis, we required the general initial condition to be of the form of nonzero Aretakis constant $H_0[\psi]$. This is equivalent to consider an initial outgoing wavepacket in the perturbation [13]. Besides the outgoing wavepacket, we can also have an initial ingoing wavepacket, which corresponds to zero Aretakis constant where the analytical argument above does not work. In this section, we will examine the behavior of massless scalar perturbations in the eRN-AdS background carefully by imposing both the outgoing and ingoing initial wavepackets.

A. Double null coordinates

With (u, v) -coordinates defined as

$$du = dt - dr_*, \quad dv = dt + dr_* \quad , \quad (13)$$

the metric (3) becomes

$$ds^2 = -f(r(u, v))dudv + r^2d\Omega \quad . \quad (14)$$

The areal radius $r(u, v)$ can be determined by solving the tortoise coordinate $r_*(r) = \frac{v-u}{2}$.

We wish a nonsingular metric at the horizon, leading us to define new coordinates as in [13], that is,

$$\begin{aligned} \frac{u}{2} &= -r_*(r_+ - U) \\ &= -\frac{R^2}{(R^2 + 6r_+^2)^2} \left[\frac{r_+^2 (R^2 + 6r_+^2)}{U} + \frac{R^4 + 7R^2r_+^2 + 14r_+^4}{\sqrt{R^2 + 2r_+^2}} \arctan \left(\frac{2r_+ - U}{\sqrt{R^2 + 2r_+^2}} \right) \right. \\ &\quad \left. + 2r_+ (R^2 + 4r_+^2) \log(-U) - r_+ (R^2 + 4r_+^2) \log(U^2 - 4r_+U + 6r_+^2 + R^2) \right]. \end{aligned} \quad (15)$$

In (U, v) -coordinates, the position of the horizon is at $U = 0$ and in the region $U < 0$ one is outside the black hole. The metric becomes

$$ds^2 = -\frac{2f(r)}{f(r_+ - U)}dUdv + r^2d\Omega^2, \quad (16)$$

where r is a function of U and v . We can expand r for small U as

$$r = r_+ - U + \frac{1}{2} \left(\frac{1}{r_+^2} + \frac{6}{R^2} \right) U^2 + \left[\left(\frac{1}{r_+^3} + \frac{4}{R^2 r_+} \right) v - \left(\frac{9}{R^4} + \frac{1}{4r_+^4} + \frac{3}{R^2 r_+^2} \right) v^2 \right] U^3 + \dots \quad (17)$$

from which it can be shown that $\frac{f(r)}{f(r_+ - U)} = 1 + \mathcal{O}(U)$ for small U . We obtain a regular analytic metric that can be defined for $U > 0$.

B. Wave equation and initial data

Defining $\phi \equiv r\psi_l$, where l is the angular index, we obtain a wave equation for ϕ in (U, v) -coordinates from the Klein-Gordon equation (4)

$$4\partial_U\partial_v\phi + \hat{V}(U, v)\phi = 0 \quad , \quad (18)$$

where the effective potential

$$\hat{V}(U, v) = \frac{2f(r)}{f(r_+ - U)} \left(\frac{f'(r)}{r} + \frac{l(l+1)}{r^2} \right). \quad (19)$$

We consider a null “initial” surface as in [13]

$$\Sigma_0 = \{U = U_0, v \geq v_0\} \cup \{U \geq U_0, v = v_0\} \quad , \quad (20)$$

and impose the following two types of initial data:

- outgoing wavepacket

$$\phi(U, v_0) = \exp\left(-\frac{(U - \mu)^2}{2\sigma^2}\right), \quad \phi(U_0, v) = 0. \quad (21)$$

- ingoing wavepacket

$$\phi(U, v_0) = 0, \quad \phi(U_0, v) = \exp\left(-\frac{(v - \mu')^2}{2\sigma'^2}\right). \quad (22)$$

We will solve the perturbation equation numerically by using the above initial conditions. In order to do the comparison with the eRN results [13], we also set $r_+ = 1, R = 1, U_0 = -0.5$ and $v_0 = 0$ in the numerical computation.

C. Algorithm of numerical method

We apply the finite difference method suggested in [20, 26] to solve the wave equation (18), which can be discretized into

$$\phi_N = \phi_E + \phi_W - \phi_S - \delta U \delta v \hat{V} \left(\frac{v_N + v_W - u_N - u_E}{4} \right) \frac{\phi_W + \phi_E}{8} + \mathcal{O}(\epsilon^4) \quad , \quad (23)$$

where points N, S, E and W form a null rectangle with relative positions as: $N : (U + \delta U, v + \delta v), W : (U + \delta U, v), E : (U, v + \delta v)$ and $S : (U, v)$. The parameter ϵ is an overall grid scalar factor, so that $\delta U \sim \delta v \sim \epsilon$.

There is one essential point we should note: the effective potential \hat{V} is positive and vanishes at the horizon, but it diverges at $r \rightarrow \infty$, which requires that ϕ vanishes at the infinity. This is the boundary condition to be satisfied by the wave equation for the scalar field in the AdS space, which is completely different from that in the asymptotically flat space. In the perturbations of the nonextreme AdS black hole, it is this difference that makes the perturbation behave differently from that in the asymptotically flat spacetime. In the following, we will examine the effective potential

effect in the perturbation in the eRN-AdS black hole and compare with that in the asymptotically flat spacetimes. In terms of the tortoise coordinate r_* , it is seen that when r tends to infinity, r_* tends to a finite constant, which is denoted as r_*^{as} . It means that our region of interest in the $(U - v)$ diagram is below the curve $v - u(U) = 2r_*^{as}$, as shown in figure (1). On this line we set $\phi = 0$, since there $r \rightarrow \infty$ and the effective potential diverges.

The inversion of the relation $r_*(r)$ needed in the evaluation of the potential $\hat{V}(U, v)$ is the most tedious part in the computation. We overcome this difficulty by employing the method suggested in [20, 27].

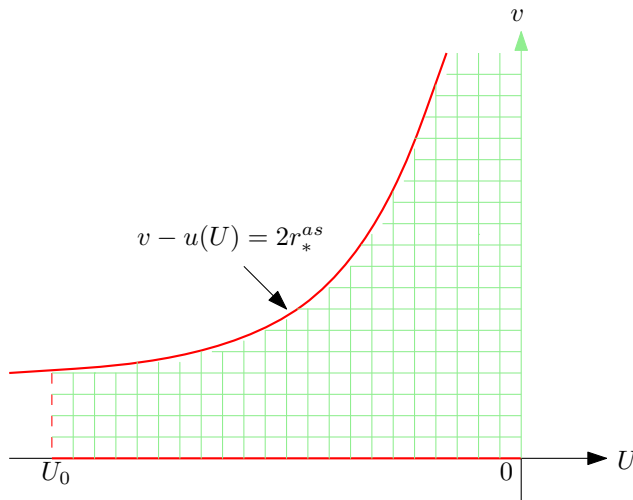


FIG. 1: Sketch graph of our interested region in (U, v) -coordinates filled with light-green mesh. Values of the scalar field on the three red lines, $v - u(U) = 2r_*^{as}$, $U = U_0$ and $v = 0$, are known according to the given initial data. In this paper, we are most interested in values of the scalar field on the horizon, which is the line $U = 0$ we show with light-green color.

D. Numerical results

1. The $l = 0$ mode

Heret we report on the numerical result of solving the wave equation (18) with $l = 0$. We define Aretakis' conserved quantity as in Eq. (7). The outgoing wave initial data (21) has nonzero $H_0[\psi]$ unless $\mu = 0$, while the ingoing wave initial data (22) and outgoing wave initial data (21) with $\mu = 0$ have zero $H_0[\psi]$. We present the results of numerical computations by using different initial

conditions in the following. To make a comparison with results in eRN case [13], we choose the same parameters for the perturbations.

1.1 Non-zero Aretakis constant

Firstl, we consider the solution with $H_0[\psi] \neq 0$, where we use the initial outgoing wavepacket (21) with $\mu \neq 0$. We have shown the instability of this type of perturbation analytically in the last section, where we assumed that ψ decays on the horizon. Here we will show that this assumption holds through numerical computation.

As in ref. [13], although we do our numerical calculations in (U, v) coordinates, we would like to display the results using (v, r) coordinates, since they correspond to the preferred coordinates, related to the symmetries of the background.

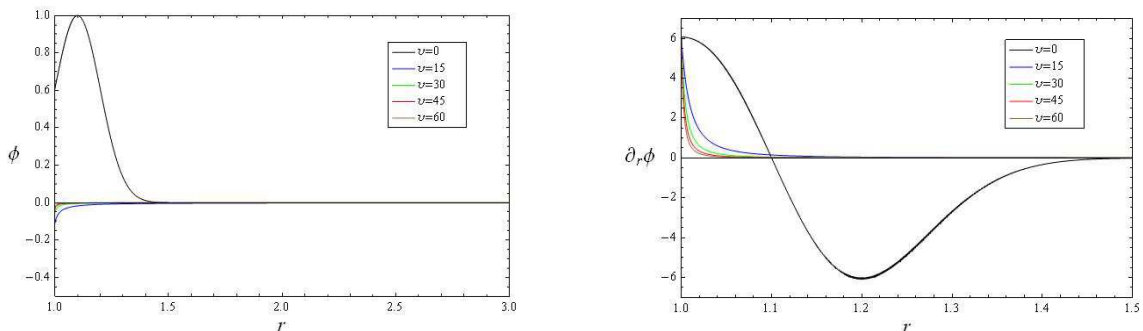


FIG. 2: Functions $\phi(v, r)$ and $\partial_r \phi(v, r)$ for $l = 0$ on fixed v slices. Seeking comparison with other results, the outgoing wave initial data is given by (21) with $(\sigma, \mu) = (0.1, -0.1)$. As we can see, ϕ decays on and outside the horizon. And $\partial_r \phi$ also decays outside the horizon, while keeping constant on the horizon. It is steeper near the horizon when v increases. Therefore, the second derivative of ϕ diverges at the horizon.

In Fig. 2, the time evolution of ϕ and $\partial_r \phi$ in (v, r) -coordinate is plotted with $(\sigma, \mu) = (0.1, -0.1)$. The figure shares some similar features in the eRN case in [13]: (1) as v increases, ϕ decays; (2) $\partial_r \phi$ also decays outside the horizon, but does not decay on the horizon; (3) Moreover, the first derivative of ϕ becomes steeper next to the horizon as v increases, indicating that $\partial_r^2 \phi$ must blow up along the horizon. Besides the similarity, we also observe the differences compared with eRN case. ϕ and $\partial_r \phi$ outside the horizon decay faster in eRN-AdS case. $\partial_r \phi$ becomes steeper more quickly near the horizon as v increases in the eRN-AdS black hole, which shows that $\partial_r^2 \phi$ on the horizon blows up more violently in the AdS background.

In Fig. 3, we have the time evolution of the field and its second derivative at the horizon. We take the constants (σ, μ) as being $(0.1, -0.1)$, $(0.05, -0.1)$, $(0.1, -0.05)$ for the sake of comparison.

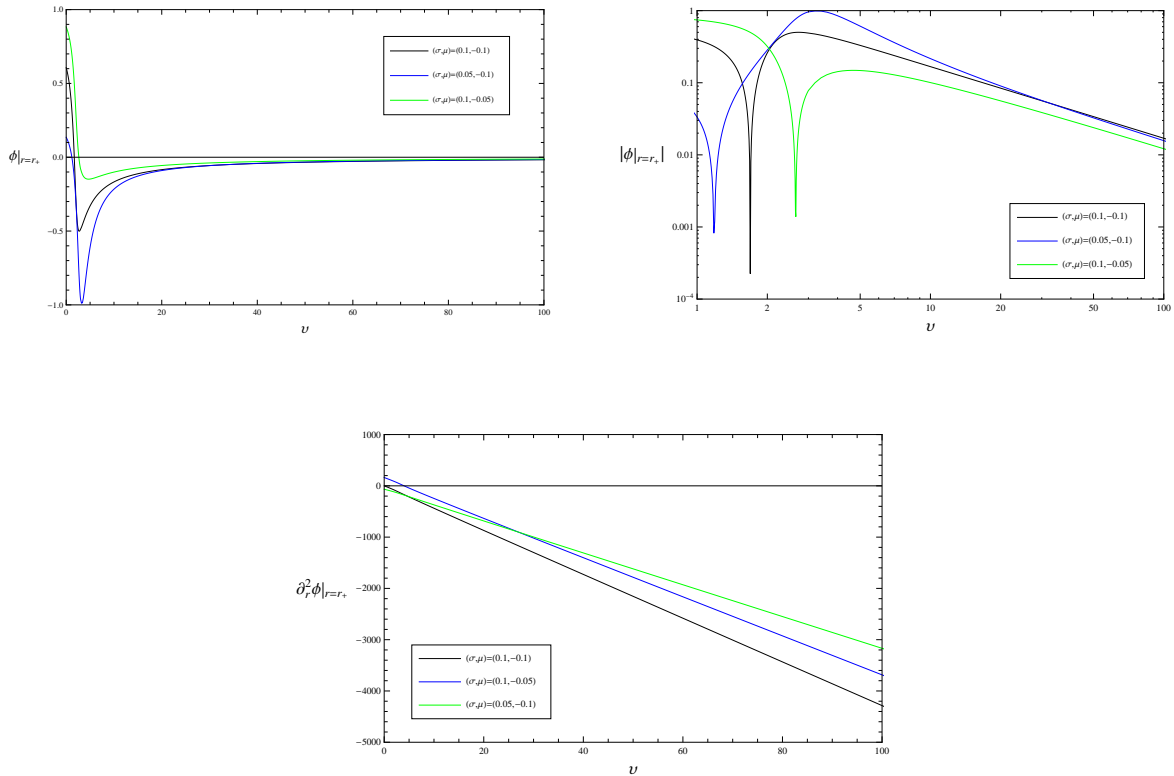


FIG. 3: Time evolution of $\phi|_{r=r_+}$ and $\partial_r^2 \phi|_{r=r_+}$ for $l = 0$ mode. We consider outgoing wave initial data (21) with various parameters: $(\sigma, \mu) = (0.1, -0.1), (0.05, -0.1), (0.1, -0.05)$. From the top-right Log-Log plot, we can see that $\phi|_{r=r_+}$ has a power-law decay. While $\partial_r^2 \phi|_{r=r_+}$ blows up as v increases, which can be seen from the bottom plot.

We can see that $\phi|_{r=r_+}$ can quickly get rid of the influence of different initial parameters and exhibit the consistent late time behavior earlier in the eRN-AdS black hole if we compare with Fig.4 of the eRN black hole case in [13]. By fitting the absolute value of $\phi|_{r=r_+}$ in the range $80 \leq v \leq 100$ to v^a , we obtain the following exponents: $a = -0.999, -1.039, -0.980$ for $(\sigma, \mu) = (0.1, -0.1), (0.05, -0.1), (0.1, -0.05)$, respectively. These results suggest that the scalar field on the horizon decays as v^{-1} at late time, which is the same as that in the eRN case [13]. The power-law decay in the late-time behavior of the massless scalar perturbation in eRN-AdS black hole is very different from results in non-extremal AdS black holes [16–18], where the late time tail exhibit exponential decay. Our result supports the argument in [25], where it was argued that when AdS black holes approach extremal limit, there is a transition from exponential decay to power-law decay. The difference in the late time perturbation indicates the dynamical difference between the extreme black hole and nonextreme black hole in AdS spacetimes. The coefficient of the power law

decay can be fitted to be $a \sim -0.28$ for all initial data we used instead of $a \sim -2$ in the eRN case. Hence, the late time behavior of $\phi|_{r=r_+}$ for the eRN-AdS black hole is

$$\phi|_{r=r_+} \sim -\frac{0.28H_0}{v} \quad v \rightarrow \infty \quad . \quad (24)$$

$\partial_r^2 \phi|_{r=r_+}$ blows up linearly as expected in the analytical study. We fit the curves of $\partial_r^2 \phi|_{r=r_+}$ to a function $cH_0v + d$ in the range $80 \leq v \leq 100$, and find the fitting parameter $c = -7.070, -7.022, -7.021$ for $(\sigma, \mu) = (0.1, -0.1), (0.05, -0.1), (0.1, -0.05)$, respectively. This suggests that $\partial_r^2 \phi|_{r=r_+} \sim -7H_0v$ at late time, which is consistent with the analytical result (11). For the eRN case [13], we can do the same fitting and find $c \sim -1$ for all the initial data. So we can see that $\partial_r^2 \phi|_{r=r_+}$ blows up faster in AdS case, which means that the horizon is more unstable in the AdS case.

1.2 Zero Aretakis constant

Now we consider perturbations with $H_0[\psi] = 0$. The case $\mu = 0$ for an ingoing or an outgoing wavepacket is here contained. The analytic proof of the instability in the last section does not work now; instead we will use a numerical calculation to study this case. To compare with the eRN case [13], we choose the same parameter spaces $(\sigma', \mu') = (3.0, 10.0)$ for the ingoing wavepacket (22), and $\sigma = 0.05, 0.1, 0.15$ and $\mu = 0$ for the outgoing wavepacket (21).

In Fig. 4, we plot the time evolutions of $\phi|_{r=r_+}$, $\partial_r^2 \phi|_{r=r_+}$ and $\partial_r^3 \phi|_{r=r_+}$. We see that $\phi|_{r=r_+}$ decays, $\partial_r^2 \phi|_{r=r_+}$ approaches to a non-zero constant and $\partial_r^3 \phi|_{r=r_+}$ blows up as v increases. These behaviors are similar to that observed in the eRN case in [13]. We see that there exists the instability even for initial data with $H_0[\psi] = 0$ in the eRN-AdS black hole.

Using the fitting method, we find that $\phi|_{r=r_+}$ has a power-law decay for the extreme AdS black hole as argued in [25], rather than an exponential decay as we observed in the nonextreme AdS hole. Fitting to the decay law v^a at late time, we find the exponent $a = -1.983$ for the ingoing wave, and $a = -1.989, -1.986, -1.984$ for the outgoing wave with $\sigma = 0.05, 0.1, 0.15$. This implies that, for $H_0[\psi] = 0$, the late time behavior of $\phi|_{r=r_+}$ is

$$\phi|_{r=r_+} \sim \frac{C}{v^2} \quad v \rightarrow \infty \quad . \quad (25)$$

This result is the same as in the eRN case [13].

Now let us take a closer look at the instability, which is shown in the late time behavior of $\partial_r^3 \phi|_{r=r_+}$. By fitting values of $|\partial_r^3 \phi|_{r=r_+}|$ to function v^a at late time, we find the fitting parameter $a = 0.979$ for the ingoing wave, and $a = 0.982, 0.980, 0.978$ for the outgoing wave with $\sigma = 0.05, 0.1, 0.15$ respectively. This confirms that $\partial_r^3 \phi|_{r=r_+}$ indeed blows up as v increases. To determine the coefficient of the linear blow up, we fit $|\partial_r^3 \phi|_{r=r_+}|$ to the function $bv + c$ for $50 \leq v \leq 100$,

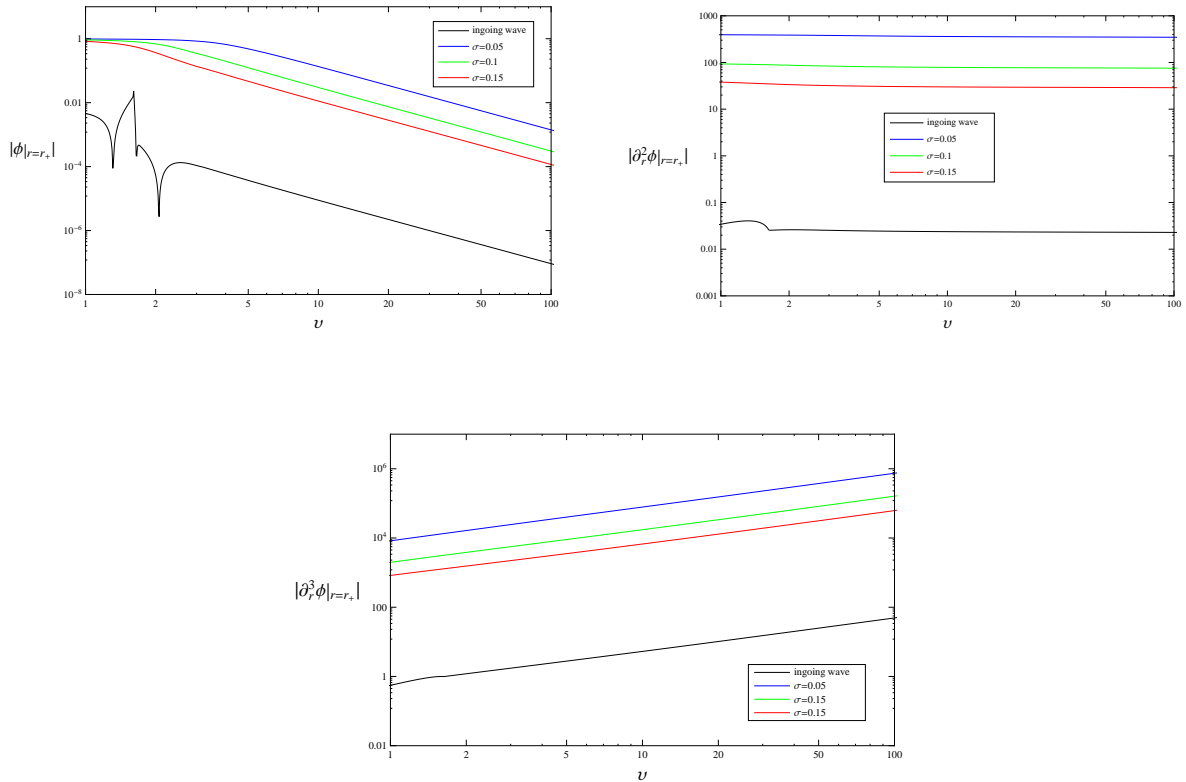


FIG. 4: Log-Log plots of time evolution of $\phi|_{r=r_+}$, $\partial_r^2 \phi|_{r=r_+}$ and $\partial_r^3 \phi|_{r=r_+}$ for $l = 0$ and $H_0 = 0$. The initial data are: $\sigma = 0.05, 0.1, 0.15$ with $\mu = 0$ and for outgoing wavepacket, while $(\sigma', \mu') = (3.0, 10.0)$ for an ingoing wavepacket. As in previous results, for large values of ν the field at the horizon decays as ν^{-2} , its second derivative at the horizon approaches a non-vanishing constant, while the third derivative diverges.

where we find $b = 0.483$ for the ingoing wave and $b = 7322.14, 1593.8, 608.642$ for the outgoing wave with $\sigma = 0.05, 0.1, 0.15$ respectively. We can also do the same fitting for the results in eRN case [13], which gives $b = 3.198$ for the ingoing wave, and $b = 921.548, 190.923, 65.965$ for the outgoing wave with $\sigma = 0.05, 0.1, 0.15$ respectively. Comparing with the eRN case, we observe that the instability is moderate for the ingoing perturbation and more violent for the outgoing perturbation in the eRN-AdS case.

2. The $l = 1$ mode

For $l = 1$ mode, we can no longer define an Aretakis constant H_1 as did in the eRN case [13]. So we can not classify perturbations according to whether H_1 is zero or not. But for convenience to do the comparison with the eRN case, we will still classify perturbations into two classes, Type

I and Type II perturbations, according to the outgoing and ingoing initial wavepackets we choose.

2.1 Type I perturbations

In this part, we consider type I perturbations, an outgoing wavepacket (21) with the same parameters as chosen in [13]: $(\sigma, \mu) = (0.1, 0), (0.1, -0.05), (0.05, 0)$. These correspond to perturbations with non-zero Aretakis constant in eRN case.

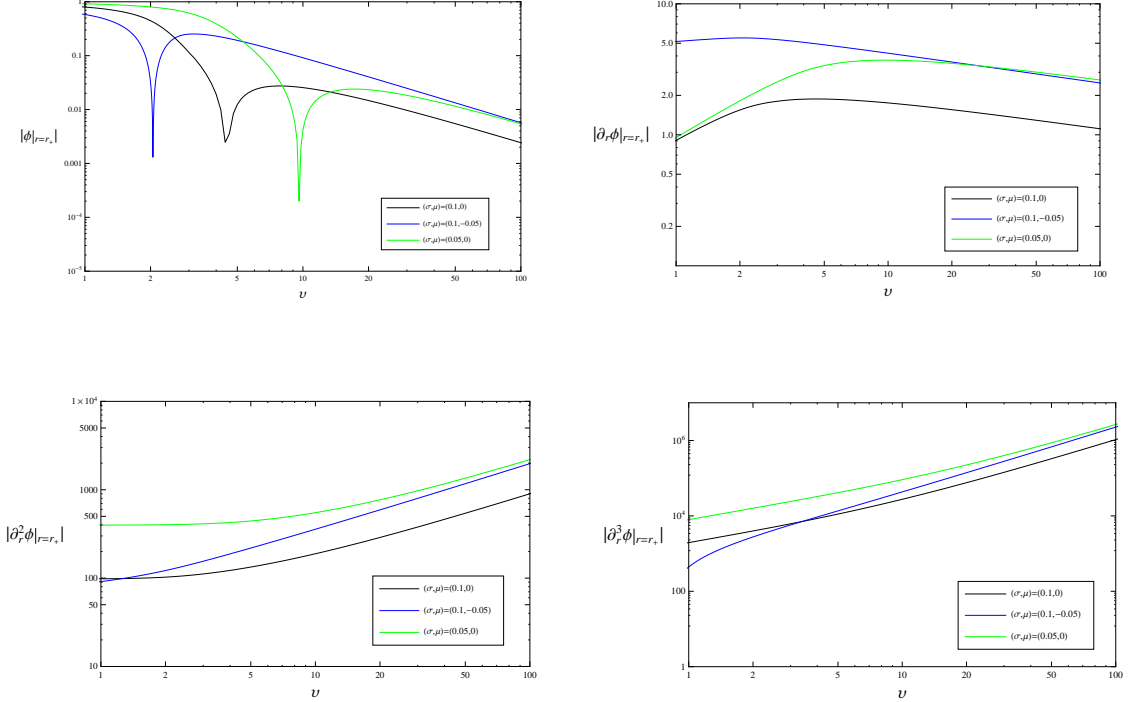


FIG. 5: Time evolution of $\phi|_{r=r_+}$, $\partial_r \phi|_{r=r_+}$, $\partial_r^2 \phi|_{r=r_+}$ and $\partial_r^3 \phi|_{r=r_+}$ for $l = 1$. We use the initial data as $(\sigma, \mu) = (0.1, 0), (0.1, -0.05), (0.05, 0)$. We can see that: $\phi|_{r=r_+}$ and $\partial_r \phi|_{r=r_+}$ exhibit a power-law decay, while $\partial_r^2 \phi|_{r=r_+}$ and $\partial_r^3 \phi|_{r=r_+}$ take a power-law blow-up. This implies that, for $l = 1$ mode, horizon instability starts to appear from the second derivative of ϕ .

In Fig. 5, we plot the time evolution of $\phi|_{r=r_+}$, $\partial_r \phi|_{r=r_+}$, $\partial_r^2 \phi|_{r=r_+}$ and $\partial_r^3 \phi|_{r=r_+}$. $\phi|_{r=r_+}$ and $\partial_r \phi|_{r=r_+}$ are shown in the first two plots in Fig. 5. They both exhibit power-law decays, but $\partial_r \phi|_{r=r_+}$ has a slower decay. Fitting the absolute value of $\phi|_{r=r_+}$ to the function v^a at late time, we find the fitting exponent $a = -1.191, -1.230, -1.127$ for $(\sigma, \mu) = (0.1, 0), (0.1, -0.05), (0.05, 0)$ respectively. This suggests that the late time behavior of $\phi|_{r=r_+}$ is

$$\phi|_{r=r_+} \sim C v^{-6/5} \quad v \rightarrow \infty, \quad (26)$$

which is very different from the result in eRN case [13], where $\phi|_{r=r_+} \sim v^{-2}$ as $v \rightarrow \infty$. Fitting

the absolute value of $\partial_r \phi|_{r=r_+}$ to v^a at late time, we find $a = -0.218, -0.229, -0.206$ for $(\sigma, \mu) = (0.1, 0), (0.1, -0.05), (0.05, 0)$ respectively.

Now we investigate the instability. We can see that the instability starts to appear in the second derivative of ϕ on the horizon. While in eRN case, the horizon instability starts to appear in the third derivative. By fitting the value of $|\partial_r^2 \phi|_{r=r_+}|$ to v^a at late time, we find the fitting parameter $a = 0.740, 0.757, 0.713$ for $(\sigma, \mu) = (0.1, 0), (0.1, -0.05), (0.05, 0)$ respectively. Fitting the value of $|\partial_r^3 \phi|_{r=r_+}|$ to v^a for $80 \leq v \leq 100$, we find $a = 1.703, 1.746, 1.645$ for $(\sigma, \mu) = (0.1, 0), (0.1, -0.05), (0.05, 0)$ respectively.

For clarity, we list all the fitting results above in Table I.

2.2 Type II perturbations

Now we consider type II perturbations, where we take an ingoing wavepacket (22) with $(\sigma', \mu') = (3.0, 10.0)$ or an outgoing wavepacket (21) with $\sigma = 0.05, 0.1$ and $\mu = \sigma \left(\sigma - \sqrt{\sigma^2 + 4r_+^2} \right) / (2r_+)$. These initial wavepackets correspond to perturbations with zero Aretakis constant cases in eRN case [13].

From Fig. 6, we can see that $\phi|_{r=r_+}$ and $\partial_r \phi|_{r=r_+}$ exhibit a power-law decay, while $\partial_r^2 \phi|_{r=r_+}$ and $\partial_r^3 \phi|_{r=r_+}$ take a power law blow-up. This implies that, for all cases we have considered here, horizon instability appears starting from the second derivative of ϕ . This is different from that in the eRN case [13], in which horizon instability starts to appear from the fourth derivative of ϕ .

Fitting the late time behavior of $\phi|_{r=r_+}, \partial_r \phi|_{r=r_+}, \partial_r^2 \phi|_{r=r_+}, \partial_r^3 \phi|_{r=r_+}$ and $\partial_r^4 \phi|_{r=r_+}$ to v^a , we can find the exponent a for these functions. We list all the fitting results in table I.

From table I, we can see that, for type II perturbations, the late time behavior of $\phi|_{r=r_+}$ is about

$$\phi|_{r=r_+} \sim C v^{-5/4} \quad v \rightarrow \infty \quad . \quad (27)$$

This is very different from eRN case [13], where $\phi|_{r=r_+} \sim v^{-3}$ as $v \rightarrow \infty$. It shows that in the eRN-AdS black hole background, the massless scalar perturbation decays much slower compared with the eRN black hole case. Moreover, we can see from the table that the late time behavior of $\partial_r^n \phi|_{r=r_+}$ takes a power-law as v^{a_0+n} with $a_0 \sim -6/5$ and $a_0 \sim -5/4$ for type I and type II perturbations, respectively. This is consistent with analytical result (12). The blow up appears earlier and more violent than that in the eRN case [13], where $\partial_r^4 \phi|_{r=r_+}$ approaches to $v^{2.7} (v^{2.8})$ in eRN-AdS while $v^2(v)$ in eRN case for type I (II) perturbations.

Comparing with $l = 0$ mode discussed in last section, the late time behavior of $\phi|_{r=r_+}$ with $l = 1$ for ingoing wave initial data takes a moderate power-law decay. This is contrary to the observation

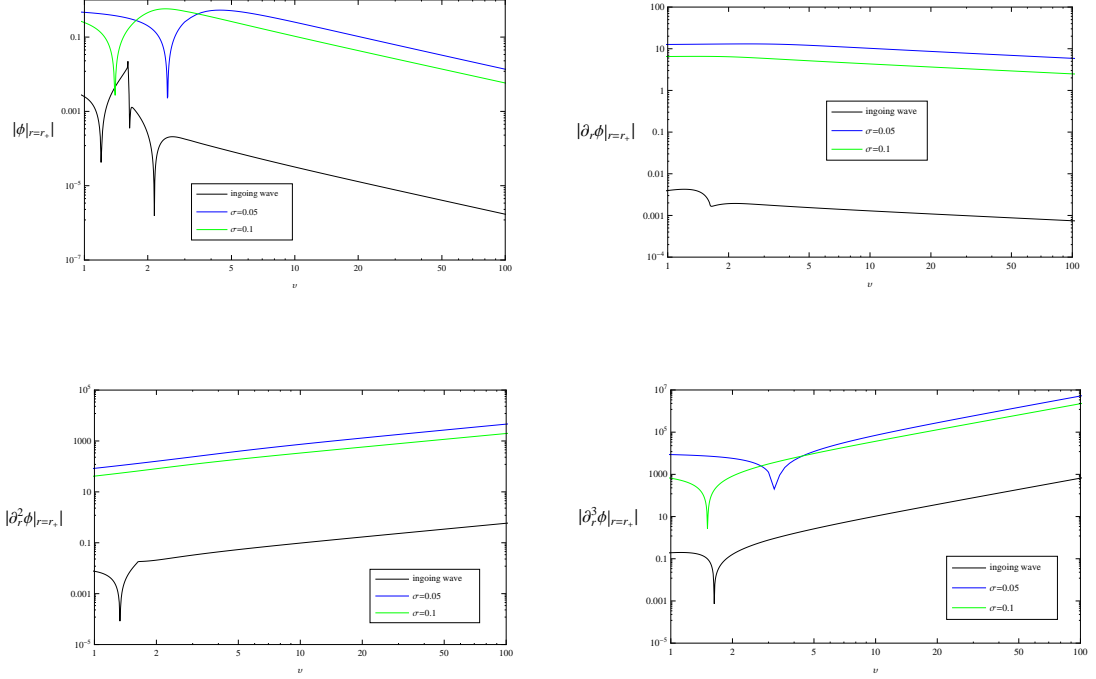


FIG. 6: Time evolution of $\phi|_{r=r_+}$, $\partial_r \phi|_{r=r_+}$, $\partial_r^2 \phi|_{r=r_+}$ and $\partial_r^3 \phi|_{r=r_+}$ for $l = 1$. For the ingoing wavepacket, the initial data takes $(\sigma', \mu') = (3.0, 10.0)$, and for the outgoing wavepacket, the initial data takes $\sigma = 0.05, 0.1$ and $\mu = \sigma \left(\sigma - \sqrt{\sigma^2 + 4r_+^2} \right) / (2r_+)$. We can see that: $\phi|_{r=r_+}$ and $\partial_r \phi|_{r=r_+}$ exhibit a power-law decay, while $\partial_r^2 \phi|_{r=r_+}$ and $\partial_r^3 \phi|_{r=r_+}$ take a power law blow-up. This also implies that, for $l = 1$ mode, horizon instability starts to appear from the second derivative of ϕ .

(σ, μ)	Type I perturbations			Type II perturbations		
	(0.1, 0)	(0.1, -0.05)	(0.05, 0)	ingoing wave	0.05	0.1
$\phi _{r=r_+}$	-1.191	-1.230	-1.127	-1.246	-1.252	-1.243
$\partial_r \phi _{r=r_+}$	-0.218	-0.229	-0.206	-0.230	-0.233	-0.234
$\partial_r^2 \phi _{r=r_+}$	0.740	0.757	0.713	0.768	0.772	0.763
$\partial_r^3 \phi _{r=r_+}$	1.703	1.746	1.645	1.770	1.781	1.762
$\partial_r^4 \phi _{r=r_+}$	2.668	2.745	2.587	2.772	2.787	2.769

TABLE I: Fitting results of the exponent a for the function v^a with $l = 1$. We fit the absolute values of ϕ and its derivative up to the fourth level to v^a for $80 \leq v \leq 100$. In type I perturbations, initial data are chosen to be $(\sigma, \mu) = (0.1, 0), (0.1, -0.05), (0.05, 0)$. In type II perturbations, parameters are chosen to be $(\sigma', \mu') = (3.0, 10.0)$ for the ingoing wave, and $\sigma = 0.05, 0.1$ and $\mu = \sigma \left(\sigma - \sqrt{\sigma^2 + 4r_+^2} \right) / (2r_+)$ for the outgoing wave. From the table, we can see that, for large v , the late time behavior of $\partial_r^n \phi|_{r=r_+}$ is about v^{a_0+n} with $a_0 \sim -6/5$ and $a_0 \sim -5/4$ for type I and type II perturbations, respectively.

in the eRN case [13], but is consistent with results in the nonextreme RN-AdS black hole [24, 25].

3. For $l > 2$ modes

We also extend our numerical calculation to the $l = 2, 3, 4$ and 5 modes to see further the effect of l on the decay law of $\phi|_{r=r_+}$ and on the blow-up behavior of $\partial_r^n \phi|_{r=r_+}$ ($n > 0$). We consider both the outgoing wave initial data and an ingoing wave initial data. We observe that the late time behavior of $\phi|_{r=r_+}$ for these modes are all power-law decay. This further confirms the argument in [25] that when the nonextreme AdS becomes extreme, the exponential decay of the perturbation will give way to the power-law decay. Also by fitting values of $\phi|_{r=r_+}$ to v^a , we can find the exponent a for all these modes, which we list in table II. We plot the results of the late time tails of ingoing wave case in fig. 7.

	$l = 0$	$l = 1$	$l = 2$	$l = 3$	$l = 4$	$l = 5$
outgoing wave	-1	-1.230	-1.563	-1.865	-2.286	-2.631
ingoing wave	-2	-1.246	-1.557	-1.926	-2.238	-2.605

TABLE II: Fitting results of the exponent a for the function v^a for different modes. We fit the absolute values of $\phi|_{r=r_+}$ to v^a for $80 \leq v \leq 100$. The parameters of the initial perturbations are chosen to be $(\sigma, \mu) = (0.1, -0.05)$ and $(\sigma', \mu') = (3.0, 10.0)$ for the outgoing and ingoing wave, respectively.

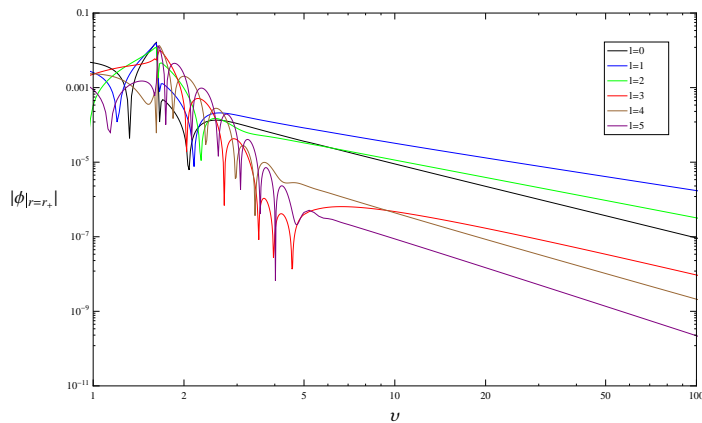


FIG. 7: Time evolution of $\phi|_{r=r_+}$ for different l for the ingoing wave. Parameters are chosen to be $(\sigma', \mu') = (3.0, 10.0)$. All these modes at late time are power-law decay. And modes with $l \geq 4$ decay faster than the $l = 0$ mode.

From table II and fig. 7, we can see that at late time: (1) For the outgoing wave with non-zero Aretakis constant H_0 , mode with higher l will decay faster; (2) For the ingoing wave (with zero Aretakis constant H_0), when $l > 0$, the first three modes with $l = 1, 2, 3$ decay slower than the fundamental mode; while when $l \geq 4$ it decays faster than the $l = 0$ mode. This implies that the decay of the massless scalar field will be dominated by the first few lower- l modes. This is in some similarity with the situation in de-Sitter black hole, where the late time behavior of massless scalar ingoing perturbations is [27, 28]

$$|\phi| \sim \begin{cases} e^{-l\kappa_c t} & l > 0 \\ |\phi_0| + |\phi_1|e^{-2\kappa_c t} & l = 0 \end{cases}, \quad (28)$$

The item κ_c is the surface gravity on the cosmological horizon and ϕ_0, ϕ_1 are some constants. In the de Sitter case, the decay law of different modes are also divided into two branches, $l = 0$ mode and $l > 0$ modes, and for $l > 2$ it decays faster than the fundamental mode.

From table I and II, we can also see that, for $l > 0$ modes, horizon instability starts to appear from the second ($l = 1, 2, 3$) or third ($l = 4, 5$) derivative of ϕ , earlier than that in the eRN case.

IV. CONCLUSIONS AND DISCUSSION

Recent studies have proved that a massless scalar field has an instability at the horizon of an extreme Reissner-Nordström black hole. Considering that a scalar field will confront different boundary conditions when it propagates in the AdS background, we have extended the stability study to extreme RN-AdS black hole. We have studied the massless scalar perturbations for different angular index. For $l = 0$ mode, we can define the Aretakis constant H_0 , and hence have shown the horizon instability analytically by assuming that the scalar field $\phi|_{r=r_+}$ on the horizon decays at late time.

Furthermore, we have applied numerical calculation and found the supporting evidence of the decay of $\phi|_{r=r_+}$. We have extended our numerical computation to the higher modes and found the consistent power-law decay of the massless scalar field perturbation. The decay of the scalar field is not exponential as observed in the nonextreme AdS black hole[16–18]. In [25] it was argued that when the nonextreme AdS black hole approaches to extreme hole, the exponential decay will give way to the power-law decay. Our numerical result for the eRN-AdS black hole have supported this argument. This is an important point, since it may lead to a departure from stability already at the nonextreme level. While we expect some kind of instability in the extreme limit, already from the very fact that the extreme limit corresponds to a zero temperature thermodynamics,

it is worthwhile checking whether the stability has stronger roots. At this point, a nonlinear approximation, or at least a backreaction calculation should be important for the clarification of the stability or instability determination. Indeed, in case the backreaction pulls the black hole out of the extreme limit, there are two choices, namely either the nonextreme limit is stable, thus backreaction stabilizes the problem, or the quasiextreme case is also unstable, and the whole black hole is unstable. Very recently, there appears a work in this direction for the eRN case [29]. It was found that generically the endpoint will be a stationary nonextreme black hole, but if there exists non-generic initial perturbations, the instability will never end. We hope that it can be extended to eRN-AdS case in near future.

The dependence of the late time tail on the angular index shown in the eRN-AdS black hole here is different from that in the eRN black hole, which reflects the influence of the spacetime on the perturbation at late time.

In the eRN-AdS black hole, we have found that when $l = 0$ the horizon instability starts to appear from the second or third derivative of the scalar field when the Aretakis constant is nonzero or zero. When $l > 0$, the horizon instability starts from the second ($l = 1, 2, 3$) or third ($l = 4, 5$) derivative of the scalar field. This is different from that in the eRN case, where the blow-up appears at higher derivative of the scalar field, especially for higher angular index case [13]. This shows that the instability in the extreme AdS black hole can happen more easily than that in the extreme asymptotically flat black hole.

Acknowledgments

This work is partially supported by the National Natural Science Foundation of China and FAPESP in Brazil.

-
- [1] T. Regge and J.A. Wheeler, *Stability of a Schwarzschild singularity*, Phys. Rev. **108** (1957) 1063.
 - [2] R.A. Konoplya and A. Zhidenko, *Quasinormal modes of black holes: from astrophysics to string theory*, Rev. Mod. Phys. **83** (2011) 793 [arXiv:1102.4014[gr-qc]].
 - [3] S. Aretakis, *Decay of axisymmetric solutions of the wave equation on extreme Kerr backgrounds*, J. Funct. Anal. **263** (2012) 2770 [arXiv:1110.2006[gr-qc]].
 - [4] S. Aretakis, *Stability and instability of extreme Reissner-Nordström black hole spacetimes for linear scalar perturbations I*, Comm. Math. Phys. **307** (2011) 17 [arXiv:1110.2007[gr-qc]].

- [5] S. Aretakis, *Stability and instability of extreme Reissner-Nordström black hole spacetimes for linear scalar perturbations II*, Ann. Henri Poincaré **8** (2011) 1491 [arXiv:1110.2009[gr-qc]].
- [6] S. Aretakis, *Horizon instability of extremal black holes*, arXiv:1206.6598[gr-qc].
- [7] P. Blue and A. Soffer, *Phase space analysis on some black hole manifolds*, J. Funct. Anal. **256** (2009) 1 [arXiv:math/0511281[math.AP]].
- [8] M. Dafermos and I. Rodnianski, *The black hole stability problem for linear scalar perturbations*, Proceedings of the 12th Marcel Grossmann meeting, Eds. T. Damour, R.T. Jantzen and R. Ruffini, World Scientific (2012) [arXiv:1010.5137[gr-qc]].
- [9] A. Strominger and C. Vafa, *Microscopic origin of the Bekenstein-Hawking entropy*, Phys. Lett. **B 379** (1996) 99 [arXiv:hep-th/9601029].
- [10] M. Guica, T. Hartman, W. Song and A. Strominger, *The Kerr/CFT Correspondence*, Phys. Rev. **D 80** (2009) 124008 [arXiv:0809.4266[hep-th]].
- [11] J. Lucietti and H.S. Reall, *Gravitational instability of an extreme Kerr black hole*, Phys. Rev. **D 86** (2012) 104030 [arXiv:1208.1437[gr-qc]].
- [12] K. Murata, *Instability of higher dimensional extreme black holes*, Class. Quant. Grav. **30** (2013) 075002 [arXiv:1211.6903[gr-qc]].
- [13] J. Lucietti, K. Murata, H.S. Reall and N. Tanahashi, *On the horizon instability of an extreme Reissner-Nordström black hole*, JHEP **1303** (2013) 035 [arXiv:1212.2557[gr-qc]].
- [14] P. Bizon and H. Friedrich, *A remark about wave equations on the extreme Reissner-Nordström black hole exterior*, Class. Quant. Grav. **30** (2013) 065001 [arXiv:1212.0729[gr-qc]].
- [15] S. Aretakis, *A note on instabilities of extremal black holes under scalar perturbations from afar*, Class. Quant. Grav. **30** (2013) 095010 [arXiv:1212.1103[gr-qc]].
- [16] G.T. Horowitz and V.E. Hubeny, *Quasinormal modes of AdS black holes and the approach to thermal equilibrium*, Phys. Rev. **D 62** (2000) 024027 [arXiv:hep-th/9909056].
- [17] G.T. Horowitz, *Comments on black holes in string theory*, Class. Quant. Grav. **17** (2000) 1107 [arXiv:hep-th/9910082].
- [18] B. Wang, C.-Y. Lin and E. Abdalla, *Quasinormal modes of Reissner-Nordström Anti-de Sitter Black Holes*, Phys. Lett. **B 481** (2000) 79 [arXiv:hep-th/0003295].
- [19] J. Bicak, *Gravitational collapse with charge and small asymmetries I. Scalar perturbations*, Gen. Rel. Grav. **3** (1972) 331.
- [20] C. Gundlach, R.H. Price and J. Pullin, *Late time behavior of stellar collapse and explosions: 1. Linearized perturbations*, Phys. Rev. **D 49** (1994) 883 [arXiv:gr-qc/9307009].
- [21] C. Gundlach, R.H. Price and J. Pullin, *Late time behavior of stellar collapse and explosions: 2. Non-linear evolution*, Phys. Rev. **D 49** (1994) 890 [arXiv:gr-qc/9307009].
- [22] L.M. Burko and A. Ori, *Late time evolution of nonlinear gravitational collapse*, Phys. Rev. **D 56** (1997) 7820 [arXiv:gr-qc/9703067].
- [23] B. Wang, C. Molina and E. Abdalla, *Evolving of a massless scalar field in Reissner-Nordström Anti-de*

- Sitter space-times*, Phys. Rev. **D 63** (2001) 084001 [arXiv:hep-th/0005143].
- [24] J.-M. Zhu, B. Wang and E. Abdalla, *Object picture of quasinormal ringing on the background of small Schwarzschild Anti-de Sitter black holes*, Phys. Rev. **D 63** (2001) 124004 [arXiv:hep-th/0101133].
- [25] B. Wang, C.-Y. Lin and C. Molina, *Quasinormal behavior of massless scalar field perturbation in Reissner-Nordström anti-de Sitter spacetimes*, Phys. Rev. **D 70** (2004) 064025 [arXiv:hep-th/0407024].
- [26] R. Gómez, J. Winicour and R. Issacson, *Evolution of scalar fields from characteristic data*, J. Comp. Phys. **98** (1992) 11.
- [27] P.R. Brady, C.M. Chambers, W.G. Laarakkers and E. Poisson, *Radiative falloff in Schwarzschild-de Sitter space-time*, Phys. Rev. **D 60** (1999) 064003 [arXiv:gr-qc/9902010].
- [28] P.R. Brady, C.M. Chambers, W. Krivan and P. Laguna, *Telling tails in the presence of a cosmological constant*, Phys. Rev. **D 55**(1997) 7538 [arXiv:gr-qc/9611056].
- [29] K. Murata, H.S. Reall and N. Tanahashi, *What happens at the horizon(s) of an extreme black hole?*, arXiv:1307.6800[gr-qc].